

Single-Molecule Manipulation in Zero-Mode Waveguides

Leonard C. Schendel, Magnus S. Bauer, Steffen M. Sedlak, and Hermann E. Gaub*


The mechanobiology of receptor–ligand interactions and force-induced enzymatic turnover can be revealed by simultaneous measurements of force response and fluorescence. Investigations at physiologically relevant high labeled substrate concentrations require total internal reflection fluorescence microscopy or zero mode waveguides (ZMWs), which are difficult to combine with atomic force microscopy (AFM). A fully automatized workflow is established to manipulate single molecules inside ZMWs autonomously with noninvasive cantilever tip localization. A protein model system comprising a receptor–ligand pair of streptavidin blocked with a biotin-tagged ligand is introduced. The ligand is pulled out of streptavidin by an AFM cantilever leaving the receptor vacant for reoccupation by freely diffusing fluorescently labeled biotin, which can be detected in single-molecule fluorescence concurrently to study rebinding rates. This work illustrates the potential of the seamless fusion of these two powerful single-molecule techniques.

1. Introduction

Total internal reflection fluorescence (TIRF) and atomic force microscopy (AFM) have previously been successfully combined to enable joined force and fluorescence spectroscopy.^[1–6] However, the necessity for a method allowing autonomous optical observation of molecules manipulated mechanically within a highly populated fluorescence environment still persists. Whereas TIRF-based techniques are capable of providing fluorescence readout, fluorophore concentration in solution did not exceed 10×10^{-9} M in these studies. This intrinsic limitation^[7] drastically lowers or completely prevents the yield of successful recording of probing and simultaneous binding events as biological processes typically take place at much higher, e.g., micromolar concentrations, due to moderate affinities (see Figure S1, Supporting Information).

By using zero mode waveguides (ZMWs) these shortcomings can be mitigated as also concentrations exceeding this limit by up to three orders of magnitude up to 20×10^{-6} M^[8] provide exceptional signal-to-noise ratios. In recent years, ZMWs have shown their great potential in observing enzyme turnover and single molecule recruitment events despite fluorophore concentrations

L. C. Schendel, M. S. Bauer, Dr. S. M. Sedlak, Prof. H. E. Gaub
Lehrstuhl für Angewandte Physik and Center for NanoScience (CeNS)
Ludwig-Maximilians-Universität München
Amalienstrasse 54, Munich 80799, Germany
E-mail: gaub@lmu.de

 The ORCID identification number(s) for the author(s) of this article can be found under <https://doi.org/10.1002/sml.201906740>.

© 2020 The Authors. Published by WILEY-VCH Verlag GmbH & Co. KGaA, Weinheim. This is an open access article under the terms of the Creative Commons Attribution License, which permits use, distribution and reproduction in any medium, provided the original work is properly cited.

DOI: 10.1002/sml.201906740

of hundreds of nanomolar^[9,10] to micromolar.^[8,11,12] Additionally, since their readout does not require a specialized microscope, ZMWs are easily and broadly applicable. ZMWs are nanometer-sized cavities within a metal cladding on a glass coverslip with aperture diameters shorter than the wavelengths of visible light. Consequently, they pose an optical barrier for incident light and thereby only an evanescent field emerges with its decay length being shorter than the height of the cavity. In turn, the illuminated volume is confined within the bottom part of the ZMW cavity, giving rise to its ability of providing exceptional signal-to-noise ratios in dense fluorescent environments.

ZMWs used in parallel are a paradigm for a high-throughput method. Here, we yet utilize single ZMWs sequentially

which allows for sensitive single molecule observation and constantly provides pristine reaction compartments. Combining ZMWs with single-molecule force spectroscopy (SMFS) conducted by using AFM creates a powerful technique for joined force and fluorescence spectroscopy despite high fluorophore concentration. It allows for mechanical manipulation of single molecules and, in addition to direct fluorescence readout, provides mechanistic insights of single molecules indicating domain unfolding, cryptic binding site opening, fingerprint unfolding or ligand dissociation.

The combined use of ZMW and AFM has already been shown feasible in proof of concept studies by using the AFM cantilever tip in surface scanning mode in order to align tip and ZMW.^[13,14] Yet, manual control, cantilever degradation, and small datasets have impeded broad applicability. After mechanical manipulation of a force-activatable kinase only a single possible binding event was reported.^[13]

In this study, a revised experimental workflow is employed to demonstrate the manipulation of single molecules in ZMWs by means of automated SMFS inside ZMWs and by the use of a well-defined receptor–ligand model system based on previous work.^[15,16] We implemented site-specific covalent immobilization for our receptor–ligand model system and added a fingerprint protein domain to have clear evidence of probing single molecules. Along with this, we chose and designed our model system to deliver a clear one-step, on–off like, fluorescence behavior. Once mechanically manipulated it provides steady fluorescence for the whole observation period. The use of a noninvasive cantilever tip localization technique and a revised fabrication of our ZMWs ensures reliable ZMW localization and precise tip placement. Additionally, we developed an all-automatic routine for cantilever tip and ZMW localization, horizontal drift correction, and autofocus, which allows

for long-term measurements and single molecule interaction yields comparable with conventional SMFS based on AFM. Furthermore, an oxygen scavenging system and antiblinking reagent guarantee steady fluorescence conditions and prevent photodamage to both dye molecules and surface proteins enabling much longer measurement durations. Through this approach, we are able to observe reoccupation of mechanically depopulated monovalent streptavidin molecules by fluorescently labeled biotin. Our results show the ease of use of sample preparation and measurements execution due to automatized and reliable localization of both cantilever tip and ZMW positions—making it possible to retrieve large datasets of simultaneous force extension and fluorescence spectroscopy events to permit the observation of rare, yet relevant, events.

2. Results and Discussion

2.1. Autonomous Probing and Noninvasive Tip Localization

A custom built TIRF AFM hybrid^[17] was used as a basis allowing for a simultaneous three laser line excitation and according fluorescence readout. Additionally, the TIRF objective can be moved by a z-piezoactuator to change the focus for tip localization and ZMW probing. The chip, which in addition to the ZMW arrays has also micrometer-sized window cut-outs (5 $\mu\text{m} \times 5 \mu\text{m}$) for tip alignment is located in between the TIRF objective to the bottom and the AFM head with cantilever to the top (Figure 1a). We chose TIRF over epifluorescence since in epi-illumination, these micrometer-sized windows would allow unobstructed light propagation through the complete height of the sample resulting in substantial photodamage of the sample.

At the beginning of a ZMW probing cycle the cantilever tip position is determined (Figure 2a) by recording the white light transillumination image of the tip above a micrometer-sized localization window. The resulting absorption profile of the tip is then fitted by a 2D Gaussian, defining via its centroid position the exact tip position relative to the frame of the optical microscope. As we had shown in a previous study, with this relatively simple technique the lateral position of the tip can be determined with nm precision.^[18] We then position the tip in close proximity to the surface (100 nm) and shift the focus plane of the objective to the very tip of the cantilever. In our previous work we kept the cantilever in contact with the glass surface during image acquisition, which may damage the tip. The improved protocol used here allows long exposure times and thus high localization accuracy without impeding cantilever functionalization by prolonging tip surface contact times. This enables reliable tip localization without interfering with the functionalization of the cantilever. Subsequently, the focus

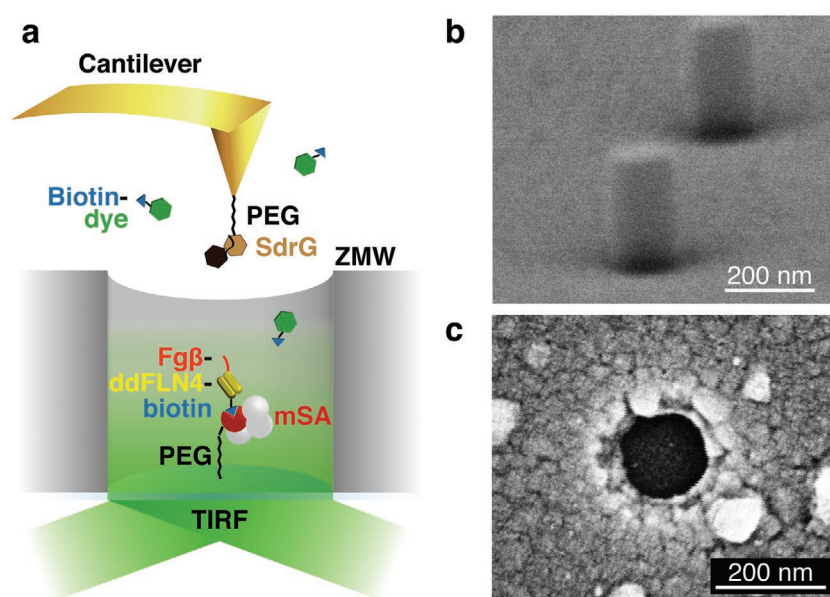


Figure 1. Experimental setup for single molecule manipulation in a ZMW. a) The bottom of a ZMW displays mSA (functional subunit in red, nonfunctional in white) on top of a polyethylene glycol (PEG) spacing layer (black). ddFLN4 (yellow) serves as a force fingerprint and is attached to mSA via biotin (blue). The Fg β -ddFLN4-biotin construct is specifically probed with an SdrG (brown) labeled AFM cantilever. Fluorescently labeled biotin (green and blue) is freely diffusing. As soon as the Fg β -ddFLN4-biotin construct is pulled out of the mSA binding pocket, the now vacant biotin binding site is occupied by freely diffusing fluorescently labeled biotin molecules. Binding events are observed via a TIRF microscope from below. b) Reflection electron microscope diagonal view of a ZMW chip after development and prior to aluminum evaporation. Pillars of cross-linked photoresist form the negative base for the ZMWs. The image shows sharp edged pillars. c) Scanning electron microscope top-down view of ZMW cavity with 80 nm radius after the experiment.

plane is shifted to the bottom of the ZMW and the positioning of the ZMW is performed using its plasmonic transmission induced by top down white light illumination. The cavity is then aligned to the cantilever tip and cantilever approach is initiated. At this point, laser illumination is turned on and the retraction force curve is recorded synchronously with the fluorescent signal (Figure 2b). After the curve was recorded a new localization is initiated and the process repeats automatically.

Our localization routine allowed to successfully align and probe ZMWs with 80 nm cavity radii (Figure S2b, Supporting Information). In order to validate successful tip placement into ZMWs, the surface contact height of the cantilever measured by the AFMs z-piezoactuator was used to calculate the height difference between ZMW aluminum surface and cavity bottom (Figure S2a, Supporting Information). For automatization, all ZMWs to be probed and a micrometer sized rectangular localization window (Figure S2c, Supporting Information) were localized at the beginning of an experiment. The preliminary positions, derived in this way, served as initial seed for ZMW localization prior to the individual probing. To allow for stable long-term probing of ZMWs, an instrument drift correction was implemented. Each time the cantilever is localized anew, the white light transmission profile of the localization window was fitted. This fit provided the center position, which was then compared with the latest derived position of the localization

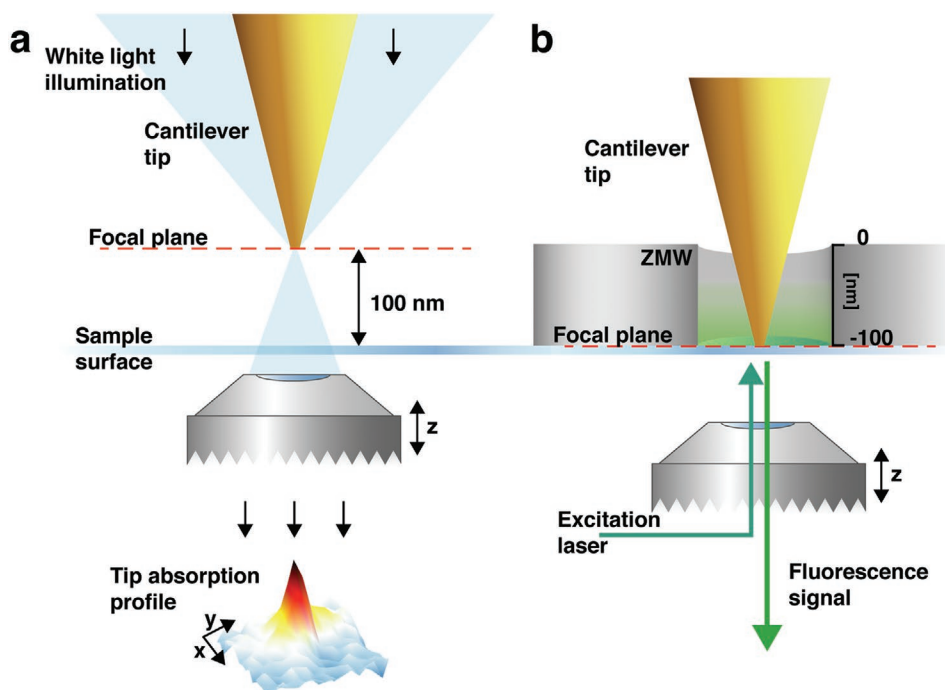


Figure 2. Precise tip localization and ZMW probing. a) Illustration of the precise cantilever tip localization procedure. The higher absorbance of light propagating through the tip is exploited which creates a distinct absorption profile. To prevent long surface contact time of the cantilever tip, acquisition of tip images is performed at a height of 100 nm above the glass surface. This allows long exposure and thus high photon yield without excessive surface contact time. The focal plane is changed by automatic movement of the objective to image the cantilever tip at 100 nm height above the surface. Tip localization is repeatedly performed during the course of an experiment. b) For ZMW probing, the objective which is mounted on a piezoactuator is vertically moved such that the focal plane coincides with the top of the glass surface plane forming the bottom of the ZMWs. After localization of the ZMW cavity by its plasmonic transmission the sample is moved horizontally to align the cantilever tip to the ZMW. Cantilever approach is initiated and laser illumination is provided through a TIRF microscope from below. During the course of an experiment, an autofocus routine corrects for vertical drift.

window. The deviation between these two values was used to correct the ZMWs preliminary positions in order to track the ZMWs despite horizontal drift. Drift in z-direction was compensated by an autofocus routine.

2.2. Blocked Monovalent Streptavidin as Force-Activated System

To test the performance of the autonomous probing setup, a monovalent streptavidin^[19] (mSA) blocked with a biotinylated ligand construct (Figure 1a) was used as a force-activatable system. With a unique cysteine^[16] localized at the C-terminus of its functional subunit, mSA was covalently attached to the glass bottom of the ZMWs. Its binding pocket was blocked with a peptide construct N-terminally featuring a short peptide from human fibrinogen $\beta^{[20]}$ (Fg β), followed by a ddFLN4 fingerprint domain^[21–23] and a C-terminal biotin. In order to force unbinding of the biotinylated construct from mSA, we used interaction of Fg β binding to the adhesin SD-repeat protein G (SdrG)^[20,24]—covalently anchored to the cantilever and much stronger than the mSA/biotin interaction. Thus, the Fg β –ddFLN4–biotin construct blocking the mSA was removed and a biotinylated dye present in excess in the measurement buffer could bind to the now vacant mSA binding pocket, as the measurement buffer of phosphate buffered saline (PBS) was

supplemented with 50×10^{-9} M Cy5-labeled biotin molecules. This binding was then recorded together with the force curve as described in the previous section. The Fg β –ddFLN4–biotin bound to the SdrG on the cantilever dissociates within tens of seconds^[25] freeing it to record the next curve. This provides cantilever regeneration in between probing for long-lasting cantilever durability. To stabilize fluorescence, the antiblinking reagent TROLOX^[26] and the oxygen scavenging compounds pyranose oxidase and catalase were added.

2.3. Fabrication of Zero Mode Waveguides

Our ZMW chips were fabricated in-house and were composed of arrays of ZMW cavities with radii of 80 nm embedded in a 100 nm thick aluminum layer (Figure 1b,c). The substrate forming the bottom consisted of borosilicate glass. Besides these nanophotonic structures, we introduced additional micrometer sized rectangular windows to our chip design (Figure S2c, Supporting Information). These windows are crucial for a combined use of AFM and ZMWs since our AFM cantilever had to be optically aligned to the frame of the optical microscope prior to alignment of the cantilever tip to ZMW cavity. To assure protein immobilization only onto the glass bottom of the ZMW cavities a material selective passivation using polyvinylphosphonic acid was applied.^[27]

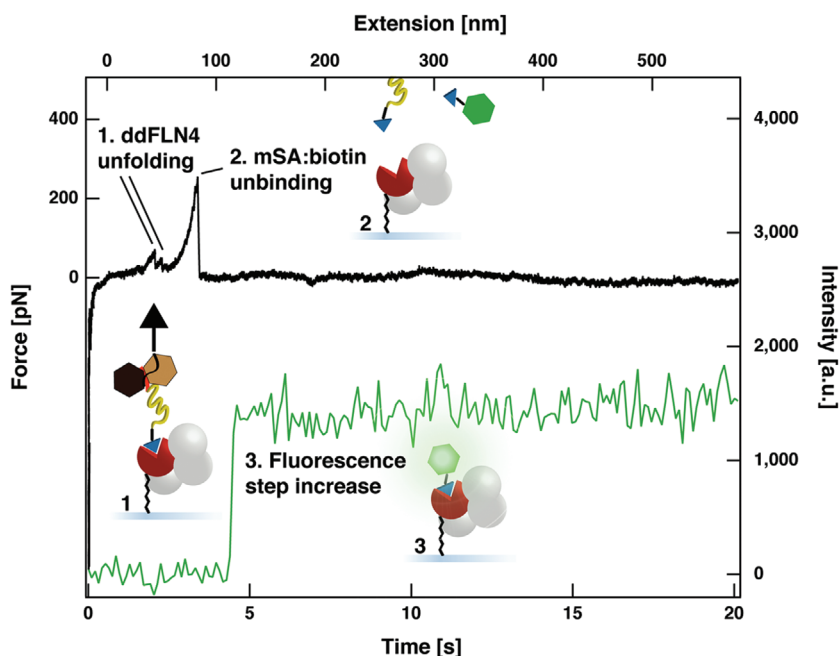


Figure 3. Force extension and fluorescence time traces for mechanical unblocking and binding event. Force versus extension curve and fluorescence intensity over time during cantilever retraction. At the zero time point the cantilever touched the bottom of the ZMW and cantilever retraction started with synchronized image acquisition. Resulting force versus extension curve (black; left and top axes) featuring the two step ddFLN4 fingerprint (yellow) unfolding (1) accompanied by mSA/biotin unbinding (2). The fluorescence signal (green; right and bottom axes) was background corrected and shows an intensity step increase (3) after the mSA/biotin unbinding. This step increase is attributed to a single labeled biotin binding to the now vacant mSA (3).

2.4. AFM-Based Single-Molecule Manipulation Experiments

We performed 505 automated mSA/biotin probing cycles inside ZMWs. In sum, 203 events constitute an interaction between cantilever tip and surface. 74 out of those probing events show successful ddFLN4 fingerprint unfolding accompanied by a biotin unbinding from mSA event (force vs extension, black graph in Figure 3). From these 74 events, 34 exhibit a single step increase (longer than 4.3 s) of fluorescence intensity without interruption after the unbinding event, seen in the fluorescence channel (intensity vs time, green graph in Figure 3). Combined graphs of force versus extension and fluorescence channel for each of the 34 events are shown in Figures S3–S8 of the Supporting Information. For these, fluorescence increases in a single step and stays high without stepwise drops in the ≈ 20 s observation time window. We attribute these 34 events to single labeled biotin binding to a mechanically vacated mSA. Upon retraction of the cantilever tip, first the ddFLN4 fingerprint unfolds (Figure 3 sequence 1) with its distinct two-step unfolding pattern. With further retraction of the cantilever tip, the biotin of the Fg β -ddFLN4-biotin construct is dissociated from mSA (Figure 3 sequence 2). This frees the formerly blocked, single binding pocket of mSA making it accessible for binding of freely diffusing Cy5-labeled biotin molecules in solution at 50×10^{-9} M, observable by fluorescence increase in a single step (Figure 3 sequence 3). We also encounter multiple unfolding events (Figure 4c,d). These feature multiple inseparable ddFLN4 unfolding and biotin unbinding events. In these

cases, we observe two consecutive steps of fluorescence intensity suggesting that we mechanically induce unblocking of multiple mSA molecules. These are then each able to bind a fluorescent biotin. In 17 cases we encountered fluorescence step increases for longer than 4 s without a prior and distinct unfolding event in the force extension channel. 6 out of these 17 events show a fluorescence step increase similar to the fluorescence traces of the 34 events but with no interaction in the force channel. They consist of a fluorescence step appearing after the AFM retraction phase (3 s) and continue to the end of the observation time window (20 s). The results of a passivation control experiment show that fluorescence steps exceeding 1 s caused by unspecific adsorption of Cy5-labeled biotin are very unlikely (cf. Table S9, Supporting Information) and cannot explain the origin of the 6 events described above.

Figure 4b shows a histogram of the time delay between biotin unbinding and the fluorescence step increase for the 34 events. The time difference between the peak force of biotin unbinding and the first time point of fluorescence step increase (Figure 4a) is plotted for each of the 34 events. Fitting a Poisson distribution for the probability of exactly one event occurring gives us a binding rate of 1.77 s^{-1} . Taking the free biotin concentration of $50 \times 10^{-9} \text{ M}$ into account yields a binding on-rate of $(3.5 \pm 0.2) \times 10^7 \text{ M}^{-1} \text{ s}^{-1}$ —in reasonable agreement with the order of magnitude reported in previous studies of the on-rate (Buranda et al.:^[28] $1.3 \times 10^7 \text{ M}^{-1} \text{ s}^{-1}$, Srisa-Art et al.:^[29] $3.0 \times 10^6 \text{ M}^{-1} \text{ s}^{-1}$ to $4.5 \times 10^7 \text{ M}^{-1} \text{ s}^{-1}$, Chivers et al.:^[30] $2.0 \times 10^7 \text{ M}^{-1} \text{ s}^{-1}$).

3. Conclusion

We have established a method to routinely manipulate individual biomolecules inside ZMWs with an AFM cantilever. We showed that we are able to reliably guide the cantilever into a multitude of ZMWs with nanometer precision and thereby probe hundreds of molecules in the course of an experiment with yields of single molecule interactions in the range of 6.7–14.7% (34 of 505 events, 74 of 505 events) being well in line with conventional AFM-based SMFS yields (8%).^[16] Due to ZMWs capability for exceptional fluorescence signal-to-noise, high fluorophore concentrations can be used. Additionally, our method drastically reduces the effort for combined SMFS and fluorescence experiments as its capability for running autonomous probing of ZMWs eliminates the need for manual control and monitoring.

Future investigation of force-mediated biochemical pathways of various proteins and enzymes, can readily be probed with our approach. Immobilization procedures can be adapted

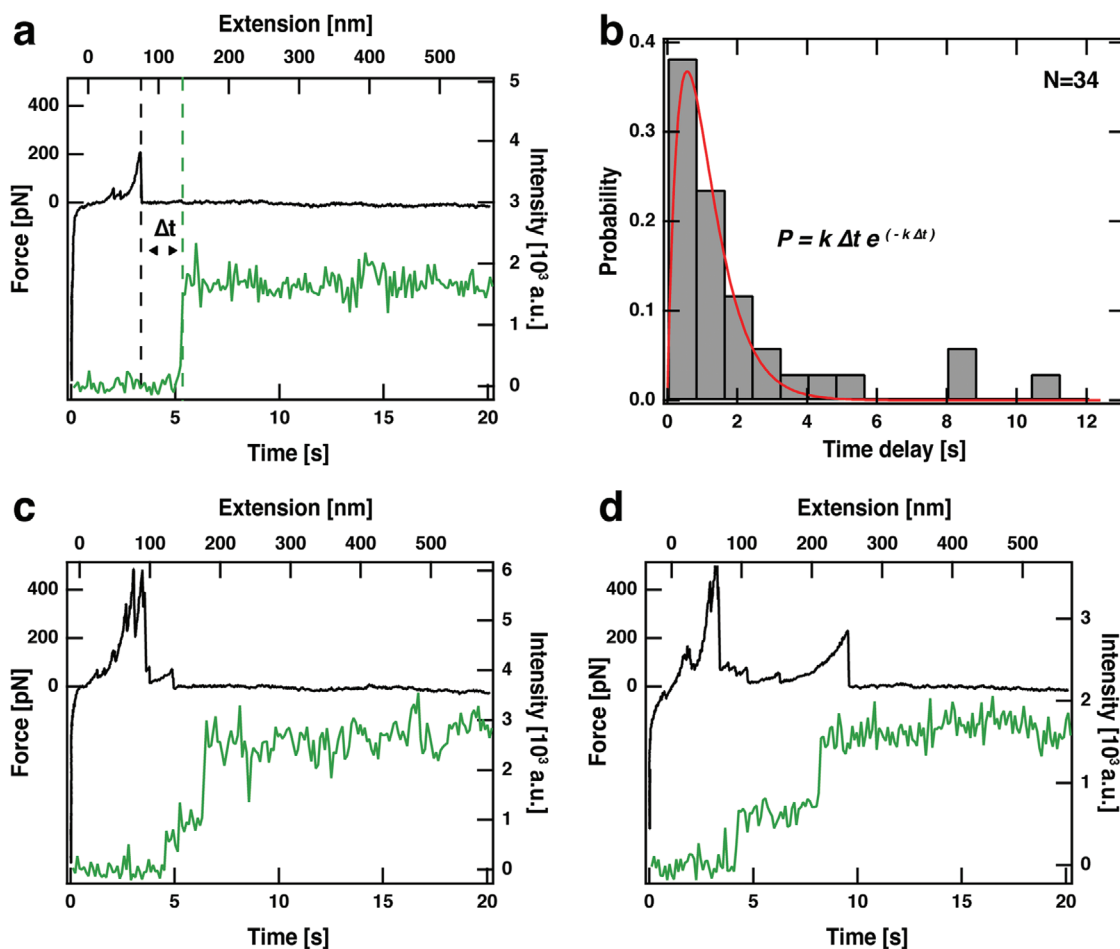


Figure 4. Time delay between biotin binding after mechanical unblocking and multiple unblocking events. a) The time to refill the empty biotin binding site in mSA was taken from the peak force (black dashed line) of biotin unbinding from mSA to the first time point of the fluorescence step increase (green dashed line). b) These time delays, time for a labeled biotin to bind to empty mSA, are plotted in a histogram and fitted by a Poisson distribution modeling the probability (P) for single event occurrence after certain time delays (Δt) with binding rate $k = 1.77 \text{ s}^{-1}$. c,d) During the experiments also multiple tether force patterns occurred with no clear ddFLN4 fingerprint, which were accompanied by multistep increase of fluorescence intensity. These were attributed to multiple biotins pulled out of multiple mSA. Thus, two labeled biotin binding events were observed, as apparent by the two-step fluorescence increase.

to site-specifically anchor other proteins to the bottom of the ZMW cavities, having the ligand fluorescently labeled in bulk solution. Thus, for example, in the field of mechanobiology, the unfolding of proteins bearing a possible cryptic binding site by SMFS and simultaneous observation of ligand binding to the subsequently exposed binding site can be studied to identify and characterize mechanosensors and to determine ligand on-rates. A system that could benefit is smooth muscle myosin light chain kinase for which experimental results recently showed new evidence that a potential force-driven activation pathway may exist.^[31] Our method could be used to observe force-induced substrate binding and enzyme turnover benefiting from ZMWs ability to observe biological processes at high, up to micromolar, fluorophore concentrations (see Figure S1, Supporting Information). For other proteins, as for example in focal adhesions, which are assumed to bear force-regulatory functions our technique can help to characterize them by providing both biochemical and biomechanical information.^[32,33] Our drift correcting, automated workflow, allows

for measuring several days without interruption. This enables probing of an even larger number of ZMWs and will thus further improve statistical power.

Regarding systems requiring higher, micromolar concentrations, the inherent limitation is set by the aspect ratio of the cantilever tip. The crucial factor is not the size of the tip itself but the diameter of the cantilever at a distance of 100 nm above the tip. The ZMWs have a height of 100 nm and a cantilever tip has to fit into the ZMW in order to probe its bottom. This limits the diameter of the ZMWs which in turn sets a limit to the concentration applicable. Thus, in order to investigate these systems, high aspect ratio cantilevers have to be used to decrease ZMW diameters on a further developed setup. Quite generally the option to mechanically trigger a biomolecular reaction and then follow its progress by fluorescent readout will allow the recording of time traces of the reaction at the level of individual molecules in a coherent and synchronized manner, in this case with maximum sensitivity and minimum background.

4. Experimental Section

ZMW Fabrication: Arrays of aluminum ZMWs and the additional structural features were patterned using negative electron-beam lithography. For this purpose, borosilicate coverslips (Menzel Gläser, Braunschweig, Germany) measuring 22 mm in diameter were thoroughly cleaned, exposed to an oxygen plasma and dried at 200 °C for 30 min. Then, they were successively spin-coated with an adhesion promoter (Surpass4000, micro resist technology, Berlin, Germany), isopropanol, and a negative tone resist (ma-N 2403, micro resist technology, Berlin, Germany). Subsequently, they were covered with a conductive silver layer. The negative pattern was then imprinted using electron beam lithography (eLINE, Raith GmbH, Dortmund, Germany). The conductive silver layer was removed using gold etchant. Following development with ma-D 525 (micro resist technology, Berlin, Germany), which exposed the cross-linked tone resist structures and pillars (Figure 1b), a 100 nm thick aluminum layer was evaporated onto the chip. Lift-off was carried out in dimethyl sulfoxide accompanied by ultrasound sonication followed by exposure to an oxygen plasma.

Besides arrays of ZMW, additional structures were incorporated in the chip design providing large (185 $\mu\text{m} \times 45 \mu\text{m}$) and smaller (5 $\mu\text{m} \times 5 \mu\text{m}$) rectangular windows for coarse and fine alignment of cantilever relative to TIRF optics.

Dimension and shape of the individual ZMWs were verified by reflection and scanning electron microscope images of both negative ZMW pillars prior aluminum deposition (Figure 1b) and completed ZMW cavities with 80 nm radius (Figure 1c).

Preparation of Proteins: The mSA molecules with its C-terminal cysteine and the Fg β -ddFLN4-ybBR construct were expressed as described by Sedlak et al.^[16] SdrG was expressed as described by Milles et al.^[20]

Surface Functionalization: To assure protein immobilization only onto the glass bottom of the ZMWs a material-selective passivation using 2% (v/v) polyvinylphosphonic acid (Polysciences Europe GmbH, Hirschberg, Germany) solution was applied.^[27] The ZMW chip was cleaned inside a UV cleaner and then immersed in 90 °C 2% (v/v) polyvinylphosphonic acid solution for 2 min. Then immersed in ultrapure H₂O, dried at 80 °C for 10 min and successively washed in ultrapure H₂O, methanol, and ultrapure H₂O. Following this, the chip was first soaked in (3-Aminopropyl)dimethylethoxysilane (ABC, Karlsruhe, Germany) 1.8% (v/v) in ethanol for 1 h, then washed in ethanol and ultrapure H₂O and baked at 80 °C for 1 h. A bifunctional polyethylene glycol (PEG) linker displaying a maleimide group was used for effective protein coupling. For this the ZMW chip was incubated with a mixture of NHS-PEG-Methyl (25 $\times 10^{-3}$ M, molecular weight 333 g mol⁻¹, Thermo Fisher Scientific, Waltham, MA, USA) and NHS-PEG-Maleimide (2.5 $\times 10^{-3}$ M, molecular weight 513.5 g mol⁻¹, Thermo Fisher Scientific, Waltham, MA, USA) in HEPES (100 $\times 10^{-3}$ M, pH 7.5).

mSA was coupled via the unique C-terminal cysteine of its single functional subunit to maleimide displayed by the PEG spacing layer in coupling buffer (50 $\times 10^{-3}$ M sodium phosphate pH 7.2, 50 $\times 10^{-3}$ M NaCl, 10 $\times 10^{-3}$ M EDTA, 0.05% (v/v) Tween 20) for 1 h and then thoroughly washed with PBS (pH 7.4, Merck, Darmstadt, Germany). The ybBR-tag of the Fg β -ddFLN4-ybBR construct was used to enzymatically couple a Coenzyme A-tagged biotin molecule utilizing the phosphopantetheinyl transferase Sfp.^[34] The enzymatic reaction was performed at 37 °C for 1 h. Two spin desalting columns (molecular weight cut-off 7 kDa, Zeba, Thermo Fisher Scientific, Waltham, MA, USA) were used to remove excess biotin. 100 $\times 10^{-9}$ M of the Fg β -ddFLN4-biotin was applied to saturate the mSA surface for 30 min. Unbound Fg β -ddFLN4-biotin was washed away with PBS. For the surface passivation control experiment the ZMW chip was treated the way described above. However, this time a different PEG linker NHS-PEG-Methyl (25 $\times 10^{-3}$ M, molecular weight 5000 g mol⁻¹, Rapp Polymere, Tübingen, Germany) in HEPES (100 $\times 10^{-3}$ M, pH 7.5) was used. Protein immobilization was omitted and surfaces were treated with 0.05% (v/v) Tween 20 prior to thoroughly washing with PBS.

Cantilever Functionalization: Cantilevers, BioLever mini (Olympus Corporation, Tokyo, Japan), displayed SdrG and were prepared as described by Sedlak et al.^[16]

Experiment Buffer: The measurement buffer was composed of PBS (pH 7.4) with 1 $\times 10^{-3}$ M TROLOX ((\pm)-6-Hydroxy-2,5,7,8-tetramethylchromane-2-carboxylic acid, Merck, Darmstadt, Germany) and an oxygen scavenger system comprised of 0.6% (w/v) D-glucose, pyranose-oxidase (7.5 U mL⁻¹, E.C. 1.1.3.10), and Catalase (1700 U mL⁻¹, E.C. 1.11.1.6) (PODCAT). Here, pyranose-oxidase proved to be more suitable than, e.g., glucose-oxidase since products of pyranose-oxidase catalyzed glucose turnover affects pH to a much less extent.^[35] TROLOX served as antiblinking reagent.^[26] Together, TROLOX and PODCAT provided stable and long-lasting fluorescence conditions with low bleaching and blinking. Cy5-labeled biotin (Click Chemistry tools, Scottsdale, USA) was used as the freely diffusing fluorescent biotin compound.

AFM-Based Single-Molecule Manipulation Experiments: The start of the retraction cycle with the start of image acquisition was synchronized by using a pulse signal output from the AFM controller to externally control the EM-CCD camera. In this way, fluorescence readout and force distance data acquisition started simultaneously. Images were taken with an exposure time of 100 ms which resulted in an effective frame rate of 106.7 ms. For ZMW probing, cantilever approach was carried out at 3000 nm s⁻¹ velocity and retraction was performed at 30 nm s⁻¹ at a sampling rate of 1500 Hz to a complete cantilever to surface distance of 550 nm. Conducting the 505 probing cycles took 5.3 h. Cy5 with a 640 nm line of a 43 mW diode laser (iChrome MLE-S, Toptica, Graefelfing, Germany) was excited by total internal reflection.

Cantilever localization was carried out in a 5 $\mu\text{m} \times 5 \mu\text{m}$ glass window within the aluminum cladding. Therefore, the cantilever was approached at 3000 nm s⁻¹ to the surface and immediately retracted at 2000 nm s⁻¹ to a cantilever to surface distance of 100 nm. Image acquisition was performed with 30 ms exposure time at an effective frame rate of 36.8 ms.

In order to align the cantilever tip to a single ZMW carrying out the autofocus routine took 8 s. Then the cantilever was moved above a localization window and cantilever tip localization was performed. The tip position was fitted and the horizontal drift was corrected using the absolute position of the localization window. This took roughly 7 s. Aligning the cantilever tip to a single ZMW was performed within 9 s. All these steps (total duration 24 s) were necessary to probe the bottom of a single ZMW. However, when probing ZMW sequentially, cantilever tip localization and autofocus were only necessary every 6th and 12th time, respectively, thereby reducing alignment times to 18 s and accelerating data acquisition. SMFS routine for the AFM controller, MFP3D (Asylum Research, Santa Barbara, CA, USA), and software for AFM-based single-molecule manipulation experiments were self-written in IGOR Pro 6 (WaveMetrics, OR, USA).

Supporting Information

Supporting Information is available from the Wiley Online Library or from the author.

Acknowledgements

The authors thank P. Altpeter and T. Nicolaus for laboratory support, L. F. Milles for substantial discussions and for providing the SdrG/Fg β -system, and E. Durner and F. Baumann for experimental setup support. This work was funded by the Deutsche Forschungsgemeinschaft (DFG, German Research Foundation) under Project-ID 201269156-SFB 1032.

Conflict of Interest

The authors declare no conflict of interest.

Author Contributions

L.C.S. performed and analyzed single-molecule force and fluorescence spectroscopy experiments. L.C.S. fabricated and analyzed ZMW chips. L.C.S. modified and enhanced experimental setup and wrote automatization software. S.M.S. and L.C.S. prepared protein constructs. H.E.G. supervised the study. L.C.S. and M.S.B. drafted the manuscript. All authors contributed with writing the final version of the manuscript.

Keywords

force activation, mechanosensing, single-molecule fluorescence, zero mode waveguides

Received: December 2, 2019

Revised: February 8, 2020

Published online: March 5, 2020

-
- [1] A. Sarkar, R. B. Robertson, J. M. Fernandez, *Proc. Natl. Acad. Sci. USA* **2004**, *101*, 12882.
- [2] S. K. Kufer, M. Strackharn, S. W. Stahl, H. Gump, E. M. Puchner, H. E. Gaub, *Nat. Nanotechnol.* **2009**, *4*, 45.
- [3] Y. He, M. Lu, J. Cao, H. P. Lu, *ACS Nano* **2012**, *6*, 1221.
- [4] K. Maki, S.-W. Han, Y. Hirano, S. Yonemura, T. Hakoshima, T. Adachi, *Sci. Rep.* **2018**, *8*, 1575.
- [5] K. R. Erlich, S. M. Sedlak, M. A. Jobst, L. F. Milles, H. E. Gaub, *Nanoscale* **2019**, *11*, 407.
- [6] R. Jöhr, M. S. Bauer, L. C. Schendel, C. Kluger, H. E. Gaub, *Nano Lett.* **2019**, *19*, 3176.
- [7] A. M. van Oijen, *Curr. Opin. Biotechnol.* **2011**, *22*, 75.
- [8] M. J. Levene, J. Korch, S. W. Turner, M. Foquet, H. G. Craighead, W. W. Webb, *Science* **2003**, *299*, 682.
- [9] J. Eid, A. Fehr, J. Gray, K. Luong, J. Lyle, G. Otto, P. Peluso, D. Rank, P. Baybayan, B. Bettman, A. Bibillo, K. Bjornson, B. Chaudhuri, F. Christians, R. Cicero, S. Clark, R. Dalal, A. deWinter, J. Dixon, M. Foquet, A. Gaertner, P. Hardenbol, C. Heiner, K. Hester, D. Holden, G. Kearns, X. Kong, R. Kuse, Y. Lacroix, S. Lin, P. Lundquist, C. Ma, P. Marks, M. Maxham, D. Murphy, I. Park, T. Pham, M. Phillips, J. Roy, R. Sebra, G. Shen, J. Sorenson, A. Tomaney, K. Travers, M. Trulson, J. Vieceli, J. Wegener, D. Wu, A. Yang, D. Zaccarin, P. Zhao, F. Zhong, J. Korch, S. Turner, *Science* **2009**, *323*, 133.
- [10] J. Chen, R. V. Dalal, A. N. Petrov, A. Tsai, S. E. O'Leary, K. Chapin, J. Cheng, M. Ewan, P.-L. Hsiung, P. Lundquist, S. W. Turner, D. R. Hsu, J. D. Puglisi, *Proc. Natl. Acad. Sci. USA* **2014**, *111*, 664.
- [11] K. T. Samiee, M. Foquet, L. Guo, E. C. Cox, H. G. Craighead, *Biophys. J.* **2005**, *88*, 2145.
- [12] T. Miyake, T. Tani, H. Sonobe, R. Akahori, N. Shimamoto, T. Ueno, T. Funatsu, I. Ohdomari, *Anal. Chem.* **2008**, *80*, 6018.
- [13] S. F. Heucke, E. M. Puchner, S. W. Stahl, A. W. Holleitner, H. E. Gaub, P. Tinnefeld, *Int. J. Nanotechnol.* **2013**, *10*, 607.
- [14] S. F. Heucke, F. Baumann, G. P. Acuna, P. M. D. Severin, S. W. Stahl, M. Strackharn, I. H. Stein, P. Altpeter, P. Tinnefeld, H. E. Gaub, *Nano Lett.* **2014**, *14*, 391.
- [15] S. M. Sedlak, M. S. Bauer, C. Kluger, L. C. Schendel, L. F. Milles, D. A. Pippig, H. E. Gaub, *PLoS One* **2017**, *12*, e0188722.
- [16] S. M. Sedlak, L. C. Schendel, M. C. R. Melo, D. A. Pippig, Z. Luthey-Schulten, H. E. Gaub, R. C. Bernardi, *Nano Lett.* **2019**, *19*, 3415.
- [17] H. Gump, S. W. Stahl, M. Strackharn, E. M. Puchner, H. E. Gaub, *Rev. Sci. Instrum.* **2009**, *80*, 063704.
- [18] F. Baumann, S. F. Heucke, D. A. Pippig, H. E. Gaub, *Rev. Sci. Instrum.* **2015**, *86*, 035109.
- [19] M. Howarth, D. J. F. Chinnapen, K. Gerrow, P. C. Dorrestein, M. R. Grandy, N. L. Kelleher, A. El-Husseini, A. Y. Ting, *Nat. Methods* **2006**, *3*, 267.
- [20] L. F. Milles, K. Schulten, H. E. Gaub, R. C. Bernardi, *Science* **2018**, *359*, 1527.
- [21] I. Schwaiger, A. Kardinal, M. Schleicher, A. A. Noegel, M. Rief, *Nat. Struct. Mol. Biol.* **2004**, *11*, 81.
- [22] L. F. Milles, E. A. Bayer, M. A. Nash, H. E. Gaub, *J. Phys. Chem. B* **2017**, *121*, 3620.
- [23] M. S. Bauer, L. F. Milles, S. M. Sedlak, H. E. Gaub, *bioRxiv* **2018**, 276444.
- [24] P. Herman, S. El-Kirat-Chatel, A. Beaussart, J. A. Geoghegan, T. J. Foster, Y. F. Dufrene, *Mol. Microbiol.* **2014**, *93*, 356.
- [25] K. Ponnuraj, M. G. Bowden, S. Davis, S. Gurusiddappa, D. Moore, D. Choe, Y. Xu, M. Hook, S. V. L. Narayana, *Cell* **2003**, *115*, 217.
- [26] T. Cordes, J. Vogelsang, P. Tinnefeld, *J. Am. Chem. Soc.* **2009**, *131*, 5018.
- [27] J. Korch, P. J. Marks, R. L. Cicero, J. J. Gray, D. L. Murphy, D. B. Roitman, T. T. Pham, G. A. Otto, M. Foquet, S. W. Turner, *Proc. Natl. Acad. Sci. USA* **2008**, *105*, 1176.
- [28] T. Buranda, G. M. Jones, J. P. Nolan, J. Keij, G. P. Lopez, L. A. Sklar, *J. Phys. Chem. B* **1999**, *103*, 3399.
- [29] M. Srisa-Art, E. C. Dyson, A. J. deMello, J. B. Edl, *Anal. Chem.* **2008**, *80*, 7063.
- [30] C. E. Chivers, E. Crozat, C. Chu, V. T. Moy, D. J. Sherratt, M. Howarth, *Nat. Methods* **2010**, *7*, 391.
- [31] F. Baumann, M. S. Bauer, M. Rees, A. Alexandrovich, M. Gautel, D. A. Pippig, H. E. Gaub, *eLife* **2017**, *6*, e26473.
- [32] V. Vogel, *Annu. Rev. Biophys. Biomol. Struct.* **2006**, *35*, 459.
- [33] M. S. Bauer, F. Baumann, C. Daday, P. Redondo, E. Durner, M. A. Jobst, L. F. Milles, D. Mercadante, D. A. Pippig, H. E. Gaub, F. Gräter, D. Lietha, *Proc. Natl. Acad. Sci. USA* **2019**, *116*, 6766.
- [34] J. Yin, P. D. Straight, S. M. McLoughlin, Z. Zhou, A. J. Lin, D. E. Golan, N. L. Kelleher, R. Kolter, C. T. Walsh, *Proc. Natl. Acad. Sci. USA* **2005**, *102*, 15815.
- [35] M. Swoboda, J. Henig, H. M. Cheng, D. Brugger, D. Haltrich, N. Plumere, M. Schlierf, *ACS Nano* **2012**, *6*, 6364.